Can the external directed edges of a complete graph form a radially symmetric field at long distance?

S. Halayka*

May 30, 2010

Abstract

Using a numerical method, the external directed edges of a complete graph are tested for their level of fitness in terms of how well they form a radially symmetric field at long distance (e.g., a test for the inverse-square law in 3D space). It is found that the external directed edges of a complete graph can very nearly form a radially symmetric field at long distance if the number of graph vertices is great enough.

1 Introduction

Complete graphs have been used to construct models of quantum gravity [1–6].

It is considered here that a complete graph G_1 consists of:

1. $n(G_1)$ vertices $V(G_1)$ that are uniformly distributed along a shell $S(G_1)$ of radius $r(G_1)$.
2. $(n(G_1)^2 - n(G_1))/2$ internal non-directed edges $I(G_1)$ (e.g., internal line segments) that join the vertices together.
3. $n(G_1)^2 - n(G_1)$ external directed edges $E(G_1)$ (e.g., external rays) that are extensions of $I(G_1)$.

See Figure 1 for a diagram of a complete graph where $n(G_1) = 5$.

It seems fundamentally important to question whether or not the external directed edges $E(G_1)$ can form a radially symmetric field at long distance.

2 Method

If the field is to be considered radially symmetric, then the following two fitness criteria must be met:

*shalayka@gmail.com

1. With regard to a second shell $S(G_2)$ of larger radius $r(G_2) > r(G_1)$, the $n(G_2) = n(G_1)^2 - n(G_1)$ vertices $V(G_2)$ corresponding to where the external directed edges $E(G_1)$ intersect with $S(G_2)$ should be uniformly distributed along $S(G_2)$.

2. The external directed edges $E(G_1)$ should be normal to $S(G_2)$ at their respective intersection vertices.

With regard to the first criterion (e.g., uniform distribution fitness), the vertices $V(G_2)$ will be compared to an equal number $n(G_3) = n(G_2)$ of vertices $V(G_3)$ that are known to be uniformly distributed along a third and final shell $S(G_3)$ of radius $r(G_3) = r(G_2)$.

The generation of $n(G_3)$ uniformly distributed vertices along a 1D shell (e.g., the Thomson problem [7] on a circle) is algorithmically simple: divide the circle's 2π radians into $n(G_3)$ equal portions and then use the polar coordinate equations to generate the $n(G_3)$ corresponding vertex positions. The generation of $n(G_3)$ uniformly distributed vertices along a 2D shell (e.g., the Thomson problem on a thin spherical shell) is not algorithmically simple: an iterative vertex repulsion code [8] was used here to generate $n(G_3)$ roughly uniformly distributed vertices.

The uniform distribution fitness test used here compares the $n(G_2)$ pairs of vertices $V(G_2)_i$, $V(G_3)_i$ by analyzing the lengths of their corresponding internal non-directed edges $I(V(G_2)_i)_j$, $I(V(G_3)_i)_j$ (e.g., where $i = \{1, 2, \ldots, n(G_2)\}$, $j = \{1, 2, \ldots, n(G_2)-1\}$). Some kind of order must be established so that a reasonable correlation exists between $I(V(G_2)_i)_j$, $I(V(G_3)_i)_j$, and so the lengths of the internal non-directed edges corresponding to each pair of vertices are placed into a pair of sorted bins before the comparison begins

$$L(I(V(G_2)_i)) = \text{sort}[\text{length}[I(V(G_2)_i)_1], \ldots, \text{length}[I(V(G_2)_i)_{(n(G_2)-1)}]], \quad (1)$$

$$L(I(V(G_3)_i)) = \text{sort}[\text{length}[I(V(G_3)_i)_1], \ldots, \text{length}[I(V(G_3)_i)_{(n(G_3)-1)}]]. \quad (2)$$

Ideally, since $V(G_3)$ are known to be uniformly distributed along $S(G_3)$, the $n(G_3)$ sorted bins $L(I(V(G_3)_i))$ should all contain identical length distributions (e.g., thus defining a single reference distribution $L(I(V(G_3)))_{\text{ref}}$). Likewise, if $V(G_2)$ are also uniformly distributed along $S(G_2)$, then the $n(G_2)$ sorted bins $L(I(V(G_2)_i))$ should also all contain length distributions that are identical to $L(I(V(G_3)))_{\text{ref}}$.

The uniform distribution fitness test used here is

$$F_D(G_1) = [0, 1] = \frac{\sum_{i=1}^{n(G_2)} \sum_{j=1}^{(n(G_2)-1)} \frac{\min[L(I(V(G_2)_i))_j, L(I(V(G_3)_i))_j]}{\max[L(I(V(G_2)_i))_j, L(I(V(G_3)_i))_j]}}{n(G_2)^2 - n(G_2)}. \quad (3)$$

It is useful to note that each internal non-directed edge is analyzed exactly twice throughout the entire test, which is why equation (3) is normalized using $n(G_2)^2 - n(G_2)$, not $(n(G_2)^2 - n(G_2))/2$.

With regard to the second criterion (e.g., normal fitness), each external directed edge $E(V(G_1)_i)_j$ corresponds to one intersection vertex $V(G_2)_k$ (e.g.,

where $i = \{1, 2, \ldots, n(G_1)\}$, $j = \{1, 2, \ldots, n(G_1) - 1\}$, $k = \{1, 2, \ldots, n(G_2)\}$). Where both $S(G_1)$ and $S(G_2)$ are centred at the coordinate system origin, the normal fitness test used here is

$$F_N(G_1) = [0, 1] = \frac{\sum_{i=1}^{n(G_1)} \sum_{j=1}^{(n(G_1)-1)} \widehat{E}(V(G_1)_i)_j \cdot \widehat{V}(G_2)_k}{n(G_2)}. \quad (4)$$

3 Results

The 1D and 2D shell fitness test results for various $n(G_1)$, $r(G_1)$, and $r(G_2)$ are listed in the following tables

Uniform distribution fitness $F_D(G_1)$ for a 1D shell of radius $r(G_1) = n(G_1)$							
$r(G_2)$ \ $n(G_1)$	2	4	8	16	32	64	128
10^3	1	0.829572	0.893257	0.946621	0.993124	0.997482	0.998891
10^{10}	1	0.827916	0.886982	0.93004	0.95885	0.976516	0.986852
10^{17}	1	0.827916	0.886982	0.93004	0.95885	0.976516	0.986852

Normal fitness $F_N(G_1)$ for a 1D shell of radius $r(G_1) = n(G_1)$							
$r(G_2)$ \ $n(G_1)$	2	4	8	16	32	64	128
10^3	1	0.999997	0.999986	0.99994	0.999752	0.998991	0.995924
10^{10}	1	1	1	1	1	1	1
10^{17}	1	1	1	1	1	1	1

Uniform distribution fitness $F_D(G_1)$ for a 2D shell of radius $r(G_1) = n(G_1)$							
$r(G_2)$ \ $n(G_1)$	2	4	8	16	32	64	128
10^3	1	0.937087	0.931829	0.974859	0.97905	0.995469	0.998372
10^{10}	1	0.937088	0.930686	0.973607	0.974738	0.994824	0.997366
10^{17}	1	0.937088	0.930686	0.973607	0.974738	0.994824	0.997366

Normal fitness $F_N(G_1)$ for a 2D shell of radius $r(G_1) = n(G_1)$							
$r(G_2)$ \ $n(G_1)$	2	4	8	16	32	64	128
10^3	1	0.999997	0.999986	0.99994	0.999752	0.998992	0.995925
10^{10}	1	1	1	1	1	1	1
10^{17}	1	1	1	1	1	1	1

4 Discussion

As the fitness test results show, the external directed edges of a complete graph can very nearly form a radially symmetric field at long distance if the number

of graph vertices is great enough. For instance, the external directed edges of a 2D shell in 3D space can very nearly reproduce the inverse-square law at long distance (e.g., field strength proportional to $1/r$).

In order to link this model to the Schwarzschild metric, consider instead a complete *bidirected* graph that consists of n vertices, $(n^2 - n)/2$ internal bidirected edges (e.g., $n^2 - n$ internal rays), and $n^2 - n$ external bidirected edges (e.g., $2(n^2 - n)$ external rays). For each of the $n^2 - n$ internal/external edge pairs there are 4 ways that interaction can occur at the corresponding vertex: internal inward, internal outward, external inward, external outward. In terms of the Planck energy E_p, it is considered here that the number of vertices per Schwarzschild black hole [9] is

$$n = \frac{E}{E_p}. \tag{5}$$

If n is great enough so that the total number of ways that interaction can occur x practically simplifies

$$x = 4(n^2 - n) \approx 4n^2, \tag{6}$$

then the black hole's Hawking temperature T, Bekenstein-Hawking entropy S_{bh}, event horizon (e.g., 2D shell) radius R_s, and time-time metric component g_{00} can be very nearly reproduced at long distance

$$T = \frac{E}{k2\pi x} \approx \frac{E}{k8\pi n^2}, \tag{7}$$

$$S_{bh} = \pi x \approx 4\pi n^2, \tag{8}$$

$$R_s = \ell_p \sqrt{x} \approx 2\ell_p n, \tag{9}$$

$$g_{00} = 1 - \frac{\ell_p \sqrt{x}}{r} \approx 1 - \frac{2\ell_p n}{r}. \tag{10}$$

The Newtonian gravitational potential $V(r)$ can be very nearly reproduced at long distance if only 1 way of interaction per internal/external edge pair is considered (e.g., external outward only)

$$\frac{V(r)}{c^2} = -\frac{\ell_p \sqrt{x/4}}{r} \approx -\frac{\ell_p n}{r}. \tag{11}$$

As visualized and discussed in [7, 9, 10], a set of n uniformly distributed vertices along a 2D shell naturally produces a triangular tessellation (e.g., a Delaunay triangulation). Where $n \gg 1$, the geometric dual of a 2D shell's triangular tessellation is a tessellation that consists primarily of hexagons (e.g., a Voronoi diagram). This is interesting to note, because in the quantum graphity model [4–6] it is considered that hexagonal tessellation is the natural tessellation of a 2D plane. If the quantum graphity model is correct, then it seems that curved and flat spacetime, or at least the tessellations naturally produced by their respective minimum energy vertex distributions, would be geometrically dual. The question of whether or not this Delaunay-Voronoi minimum energy vertex distribution duality would also apply to dimensions $\mathrm{D} > 2$ is left for future

consideration (e.g., does the geometric dual of an irregular but roughly uniform tetrahedral tessellation [11] produce the minimum energy vertex distribution within flat 3D space?). See [12–24] for further information on the application of Delaunay-Voronoi tessellations.

See [25] for the fitness test C++ code and expanded table data. In the fitness test code, the iterative vertex repulsion code [8] has been modified to use the Mersenne Twister pseudorandom number generator [26] in conjunction with the sphere point picking algorithm discussed in [27]. The fitness test code also uses a modified version of the ray-shell intersection code given in [28].

References

[1] Antonsen F. Random graphs as a model for pregeometry. (1994) Int J Theor Phys 33: 1189-1205

[2] Gibbs PE. Event-Symmetric Physics. (1995) arXiv:hep-th/9505089v1

[3] Gibbs PE. The Small Scale Structure of Space-Time: A Bibliographical Review. (1995) arXiv:hep-th/9506171v2

[4] Konopka T, Markopoulou F, Smolin L. Quantum Graphity. (2006) arxiv:hep-th/0611197

[5] Konopka T, Markopoulou F, Severini S. Quantum Graphity: a model of emergent locality. (2008) arXiv:0801.0861v2 [hep-th]

[6] Markopoulou F. Space does not exist, so time can. (2008) FQXi 'The Nature of Time' Essay Contest, arXiv:0909.1861v1 [gr-qc]

[7] Cecka C, Bowick MJ, Middleton AA. Thomson problem @ S.U., Syracuse University. (2010) `http://thomson.phy.syr.edu/thomsonapplet.htm`

[8] Bulatov V. Vertex repulsion code. (1996) `http://www.math.niu.edu/~rusin/known-math/96/repulsion`

[9] Misner CW, Thorne KS, Wheeler JA. Gravitation, chapters 12, 31, and 42. (1973) ISBN: 978-0716703440

[10] McDonald JR, Miller WA. A Discrete Representation of Einstein's Geometric Theory of Gravitation: The Fundamental Role of Dual Tessellations in Regge Calculus. (2008) arXiv:0804.0279v1 [gr-qc]

[11] Yan DM, Wang W, Lévy B, Liu Y. Efficient Computation of 3D Clipped Voronoi Diagram, subfigures 3(c) and 3(d). (2010) GMP 2010 Conference Proceedings

[12] CGAL, Computational Geometry Algorithms Library. (2010) `http://www.cgal.org`

[13] The Geometry Center, The University of Minnesota. Qhull v2010.1 (2010) http://www.qhull.org

[14] Si H. TetGen – A Quality Tetrahedral Mesh Generator and a 3D Delaunay Triangulator. (2009) http://tetgen.berlios.de/

[15] Rycroft CH. Voro++. (2008) http://math.lbl.gov/voro++/

[16] McDonald JR, Miller WA. Coupling Non-Gravitational Fields with Simplicial Spacetimes. (2010) arXiv:1002.5001v2 [gr-qc]

[17] Rapaport DC. Hexagonal convection patterns in atomistically simulated fluids. (2005) arXiv:cond-mat/0508189v2 [cond-mat.other]

[18] Slotterback S, Toiya M, Goff L, Douglas JF, Losert W. Correlation between Particle Motion and Voronoi-Cell-Shape Fluctuations during the Compaction of Granular Matter. (2008) Phys Rev Lett 101

[19] Grise G, Meyer-Hermann M. Towards Sub-cellular Modeling with Delaunay Triangulation. (2010) Math Model Nat Phenom 5, No. 1: 224-238

[20] Meyer-Hermann M. Delaunay-Object-Dynamics: cell mechanics with a 3D kinetic and dynamic weighted Delaunay-triangulation. (2008) Curr Top Dev Biol 81: 373-99

[21] Walter M, Fournier A, Menevaux D. Integrating Shape and Pattern in Mammalian Models. (2001) SIGGRAPH 2001

[22] Hasegawa M, Tanemura M. On the pattern of space division by territories. (1976) Ann Inst Statist Math 28 B: 509-519

[23] Einasto J. Has the Universe a honeycomb structure? (1997) The Eighth Marcel Grossmann Meeting, arXiv:astro-ph/9711320v1

[24] Einasto J. The structure of the Universe on 100 Mpc Scales. (2000) The Ninth Marcel Grossmann Meeting, arXiv:astro-ph/0011334v1

[25] Halayka S. Fitness test C++ code v3.0. (2010) http://completegraph-rays.googlecode.com/files/rays_3.0.zip

[26] Saito M, Matsumoto M, Hiroshima University. SIMD-oriented Fast Mersenne Twister ("SFMT") v1.3.3. (2006) http://www.math.sci.hiroshima-u.ac.jp/~m-mat/MT/SFMT/

[27] Weisstein EW. Sphere Point Picking. From MathWorld–A Wolfram Web Resource. (2010) http://mathworld.wolfram.com/SpherePointPicking.html

[28] Dunn F, Parberry I. 3D Math Primer for Graphics and Game Development, chapter 13.12. (2002) ISBN: 978-1556229114

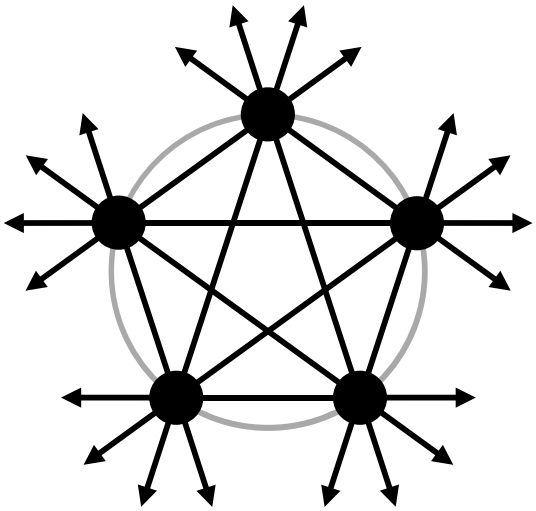

Figure 1: A complete graph G_1, where $n(G_1) = 5$ vertices $V(G_1)$ (e.g., black disks) are uniformly distributed along a 1D shell $S(G_1)$ (e.g., a gray circle). There are $(n(G_1)^2 - n(G_1))/2 = 10$ internal non-directed edges $I(G_1)$ (e.g., black internal line segments), and $n(G_1)^2 - n(G_1) = 20$ external directed edges $E(G_1)$ (e.g., black external rays). Where $i = \{1, 2, \ldots, n(G_1)\}$, $j = \{1, 2, \ldots, n(G_1) - 1\}$, each vertex $V(G_1)_i$ corresponds to $n(G_1) - 1 = 4$ internal non-directed edges $I(V(G_1)_i)_j$ and $n(G_1) - 1 = 4$ external directed edges $E(V(G_1)_i)_j$.